

Setting the physical scale of dimensional reduction in causal dynamical triangulations

Joshua H. Cooperman^{1,2} and Manuchehr Dorghabekov^{2,3}

¹*Department of Physics and Astronomy, Bucknell University, Lewisburg, Pennsylvania, United States*

²*Physics Program, Bard College, Annandale-on-Hudson, New York, United States**

³*Applied Mathematics and Informatics Program, American University of Central Asia, Bishkek, Kyrgyz Republic**

May 30, 2019

Abstract

Within the causal dynamical triangulations approach to the quantization of gravity, striking evidence has emerged for the dynamical reduction of spacetime dimension on sufficiently small scales. Specifically, the spectral dimension decreases from the topological value of 4 towards a value near 2 as the scale being probed decreases. The physical scales over which this dimensional reduction occurs have not previously been ascertained. We present and implement a method to determine these scales in units of either the Planck length or the quantum spacetime geometry’s effective de Sitter length. We find that dynamical reduction of the spectral dimension occurs over physical scales of the order of 10 Planck lengths, which, for the numerical simulation considered below, corresponds to the order of 10^{-1} de Sitter lengths.

Introduction—Studying the nonperturbative quantization of general relativity afforded by causal dynamical triangulations, Ambjørn, Jurkiewicz, and Loll made a striking discovery: the effective dimension of quantum spacetime geometry dynamically reduces to a value near 2 on sufficiently small scales [8]. This phenomenon—dynamical dimensional reduction—has been independently confirmed within causal dynamical triangulations [22] and subsequently discovered within other approaches to quantum gravity [14].

Ambjørn, Jurkiewicz, and Loll performed numerical measurements of the spectral dimension, a scale-dependent measure of dimensionality as determined by a diffusing random walker. Their measurements yielded the spectral dimension of quantum spacetime geometry as a function of diffusion time, namely the number of steps in the diffusion process. Shorter walks typically probe smaller scales, and longer walks typically probe larger scales, but there is no *a priori* connection between diffusion time and any physical scale. One is thus left pondering the question ‘Over what physical scales does dynamical reduction of the spectral dimension occur?’.

After briefly reviewing the formalism of causal dy-

namical triangulations, the definition of the spectral dimension, and the phenomenology of the former within the latter, we present and implement a method for setting the physical scales of dynamical dimensional reduction. Our method proceeds in two successive steps: we first establish the equivalent of the diffusion time in units of the lattice spacing, and we then establish the equivalent of the lattice spacing in units of either the Planck length or the quantum spacetime geometry’s effective de Sitter length. We find that the spectral dimension begins to reduce at a physical scale of 40 Planck lengths or 0.34 de Sitter lengths and continues to reduce at least to a physical scale of 10 Planck lengths or 0.10 de Sitter lengths. Interestingly, this quantum-gravitational phenomenon occurs on physical scales more than an order of magnitude above the Planck length.

Causal dynamical triangulations—Within a path integral quantization of general relativity, one formally defines a probability amplitude $\mathcal{A}[\gamma]$ by the equation

$$\mathcal{A}[\gamma] = \int_{\mathbf{g}|\partial\mathcal{M}=\gamma} d\mu(\mathbf{g}) e^{iS_{\text{EH}}[\mathbf{g}]/\hbar} : \quad (1)$$

integrate over all spacetime metric tensors \mathbf{g} , inducing the metric tensor γ on the boundary $\partial\mathcal{M}$ of the spacetime manifold \mathcal{M} , weighting each by the

*Affiliation when we initiated the research reported herein

product of a measure $d\mu(\mathbf{g})$ and the exponential of $\frac{i}{\hbar}$ times the Einstein-Hilbert action $S_{\text{EH}}[\mathbf{g}]$. Within the causal dynamical triangulations approach to this quantization [4–6, 10], one instead considers a lattice-regularized probability amplitude $\mathcal{A}_\Sigma[\Gamma]$ given by the equation

$$\mathcal{A}_\Sigma[\Gamma] = \sum_{\substack{\mathcal{T}_c \cong \Sigma \times [0,1] \\ \mathcal{T}_c|_{\partial\mathcal{T}_c} = \Gamma}} \mu(\mathcal{T}_c) e^{i\mathcal{S}_R[\mathcal{T}_c]/\hbar} \quad (2)$$

sum over all causal triangulations \mathcal{T}_c of spacetime topology $\Sigma \times [0, 1]$, inducing the triangulation Γ on the boundary $\partial\mathcal{T}_c$, weighting each by the product of a measure $\mu(\mathcal{T}_c)$ and the exponential of $\frac{i}{\hbar}$ times the Regge action $\mathcal{S}_R[\mathcal{T}_c]$. A causal triangulation \mathcal{T}_c is a piecewise-Minkowski simplicial manifold admitting a global foliation by spacelike hypersurfaces all of the chosen topology Σ . In figure 1 we depict part of a 2-dimensional causal triangulation. One con-

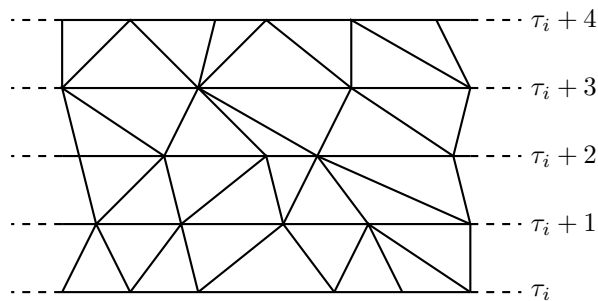


Figure 1: Part of a 2-dimensional causal triangulation with the discrete time coordinate τ labeling five consecutive leaves of its distinguished foliation.

structs a causal triangulation by appropriately gluing together N_D D -simplices, each a simplicial piece of D -dimensional Minkowski spacetime with spacelike edges of invariant length squared a^2 and timelike edges of invariant length squared $-\alpha a^2$. a is the lattice spacing, and α is a positive constant. As figure 1 shows, these D -simplices assemble such that they generate a distinguished spacelike foliation, its leaves labeled by a discrete time coordinate τ . There are $D + 1$ types of D -simplices; we distinguish these types with an ordered pair (p, q) , its entries indicating the numbers of vertices on initial and final adjacent leaves.

The foliation enables a Wick rotation of a causal triangulation from Lorentzian to Euclidean signature, achieved by analytically continuing α to $-\alpha$ through the lower half complex plane. The probability amplitude (2) transforms accordingly into the partition

function

$$\mathcal{Z}_\Sigma[\Gamma] = \sum_{\substack{\mathcal{T}_c \cong \Sigma \times [0,1] \\ \mathcal{T}_c|_{\partial\mathcal{T}_c} = \Gamma}} \mu(\mathcal{T}_c) e^{-\mathcal{S}_R^{(E)}[\mathcal{T}_c]/\hbar} \quad (3)$$

in which $\mathcal{S}_R^{(E)}[\mathcal{T}_c]$ is the resulting Euclidean Regge action. As in several past studies, we take Σ to be the 2-sphere topology, and we periodically identify the temporal interval $[0, 1]$. For these choices

$$\mathcal{S}_R^{(E)}[\mathcal{T}_c] = -k_0 N_0 + k_3 N_3 \quad (4)$$

in which k_0 and k_3 are specific functions of the bare Newton constant, the bare cosmological constant, α , and a . We consider the test case of three spacetime dimensions so that the computations required for the analysis presented below are somewhat less intensive. This analysis carries over straightforwardly to the realistic case of four spacetime dimensions, and we fully expect its results to carry over as well since these two cases possess essentially all of the same phenomenology [1, 3, 7–9, 11, 12, 18–22].

We numerically study the partition function (3) for the action (4) (at fixed numbers N_3 of 3-simplices and T of spacelike leaves) using standard Markov chain Monte Carlo methods. This partition function exhibits two phases of quantum spacetime geometry. We consider exclusively the so-called de Sitter phase, the physical properties of which we discuss below. One ascertains these physical properties by measuring observables $\mathcal{O}_{\mathcal{T}_c}$, specifically, their expectation values

$$\mathbb{E}[\mathcal{O}] = \frac{1}{\mathcal{Z}[\Gamma]} \sum_{\substack{\mathcal{T}_c \cong \Sigma \times [0,1] \\ \mathcal{T}_c|_{\partial\mathcal{T}_c} = \Gamma}} \mu(\mathcal{T}_c) e^{-\mathcal{S}_{\text{cl}}^{(E)}[\mathcal{T}_c]/\hbar} \mathcal{O}_{\mathcal{T}_c} \quad (5)$$

in the quantum state defined by this partition function, which we approximate by their averages

$$\langle \mathcal{O} \rangle = \frac{1}{N(\mathcal{T}_c)} \sum_{j=1}^{N(\mathcal{T}_c)} \mathcal{O}_{\mathcal{T}_c^{(j)}} \quad (6)$$

over an ensemble of $N(\mathcal{T}_c)$ causal triangulations generated by our Markov chain Monte Carlo algorithm.

Ultimately, one aims to learn about the probability amplitudes (1) both by taking a continuum limit in which the lattice regularization is removed *via* a nontrivial ultraviolet fixed point and by returning from Euclidean to Lorentzian signature *via* an Osterwalder-Schrader-type theorem.

Spectral dimension—The spectral dimension measures the dimensionality of a space as experienced by a random walker diffusing through this space. Taking

this space to be a Wick-rotated causal triangulation \mathcal{T}_c , the spectral dimension is specifically defined as follows [8, 9, 12].

The integrated discrete diffusion equation

$$\begin{aligned} \mathcal{K}_{\mathcal{T}_c}(s, s', \sigma) &= (1 - \varrho)\mathcal{K}_{\mathcal{T}_c}(s, s', \sigma - 1) \\ &+ \frac{\varrho}{N(\mathcal{N}_s(1))} \sum_{s'' \in \mathcal{N}_s(1)} \mathcal{K}_{\mathcal{T}_c}(s'', s', \sigma - 1) \end{aligned} \quad (7)$$

governs the random walker’s diffusion. The heat kernel element $\mathcal{K}_{\mathcal{T}_c}(s, s', \sigma)$ gives the probability of diffusion from D -simplex s to D -simplex s' (or *vice versa*) in σ diffusion time steps. $\mathcal{K}_{\mathcal{T}_c}(s, s', \sigma)$ is simply the weighted average of the probability to have diffused from s to s' in $\sigma - 1$ steps—the first term on the right hand side of equation (7)—and the probability to diffuse from a D -simplex s'' in the set $\mathcal{N}_s(1)$ of nearest neighbors to s in σ steps—the second term on the right hand side of equation (7). The diffusion constant ϱ characterizes the dwell probability of a step in the diffusion process. By averaging $\mathcal{K}_{\mathcal{T}_c}(s, s', \sigma)$ for $s = s'$ over all $N_s(\mathcal{T}_c)$ D -simplices in \mathcal{T}_c , one arrives at the return probability (or heat trace):

$$\mathcal{P}_{\mathcal{T}_c}(\sigma) = \frac{1}{N_s(\mathcal{T}_c)} \sum_{s=1}^{N_s(\mathcal{T}_c)} \mathcal{K}_{\mathcal{T}_c}(s, s, \sigma). \quad (8)$$

As its name implies, $\mathcal{P}_{\mathcal{T}_c}(\sigma)$ —and, subsequently, the spectral dimension—derives from random walks that return to their starting D -simplices.

One now defines the spectral dimension $\mathcal{D}_s^{(\mathcal{T}_c)}(\sigma)$ as the power with which $\mathcal{P}_{\mathcal{T}_c}(\sigma)$ scales with σ multiplied by -2 :

$$\mathcal{D}_s^{(\mathcal{T}_c)}(\sigma) = -2 \frac{d \ln \mathcal{P}_{\mathcal{T}_c}(\sigma)}{d \ln \sigma} \quad (9)$$

for a suitable discretization of the logarithmic derivative. Equation (9) provides a measure of a causal triangulation’s dimensionality as a function of σ . We approximate the expectation value $\mathbb{E}[\mathcal{D}_s(\sigma)]$ of $\mathcal{D}_s^{(\mathcal{T}_c)}(\sigma)$ by the ensemble average $\langle \mathcal{D}_s(\sigma) \rangle$. We follow the methods of [16] in estimating $\langle \mathcal{D}_s(\sigma) \rangle$ and its error.

In figure 2 we display $\langle \mathcal{D}_s(\sigma) \rangle$ for an ensemble of causal triangulations within the de Sitter phase characterized by $k_0 = 1$ and $N_3 = 30850$ for $\varrho = 0.8$. We study this ensemble throughout the paper.¹ The plot in figure 2 displays the characteristic behavior

¹The analysis that we describe below, particularly its first part, is computationally intensive; accordingly, with the computing resources available to us, we have not yet analyzed ensembles characterized by larger values of N_3 . Cooperman has demonstrated that this ensemble provides physically reliable results for the spectral dimension [18].

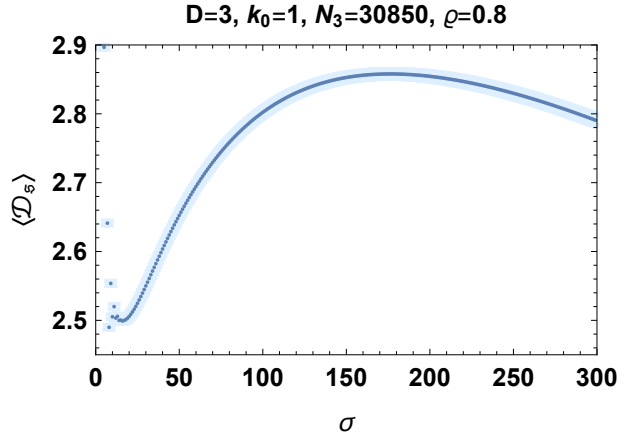


Figure 2: The ensemble average spectral dimension $\langle \mathcal{D}_s \rangle$ as a function of the diffusion time σ (in blue). Each point’s vertical extent (in light blue) indicates its statistical error.

of $\langle \mathcal{D}_s(\sigma) \rangle$ within this phase. $\langle \mathcal{D}_s(\sigma) \rangle$ first increases monotonically from a value of approximately 2.5 to a value of approximately 2.86 and then decreases monotonically from a value of approximately 2.86 (eventually) towards a value of 0. This monotonic rise, followed in reverse, is the phenomenon of dynamical reduction of the spectral dimension; the monotonic fall results from the quantum geometry’s large-scale positive curvature [12]. Finite-size effects depress the maximum of $\langle \mathcal{D}_s(\sigma) \rangle$ below the topological value of 3 [18].

Question—The diffusion time σ is simply the parameter that enumerates the random walker’s steps. For smaller values of σ , the random walker typically probes smaller physical scales, and, for larger values of σ , the random walker typically probes larger physical scales. The quantitative correspondence between σ and the physical scales being probed depends on the space through which the random walker diffuses. We propose a method to determine this correspondence for an ensemble of causal triangulations within the de Sitter phase. We implement this method to set the physical scales characterizing the phenomenology of the ensemble average spectral dimension $\langle \mathcal{D}_s(\sigma) \rangle$ within the de Sitter phase. Specifically, we determine the interval of physical scales over which dynamical reduction occurs and the physical scale at which $\langle \mathcal{D}_s(\sigma) \rangle$ coincides with the topological dimension D .

Methods—Our method is conceptually straightforward. First we directly determine the average geodesic distance in units of the lattice spacing a traversed by the random walker for walks that return in

σ diffusion time steps. Then we employ the analysis of [3] to express the lattice spacing a in units of either the Planck length ℓ_P or the quantum spacetime geometry's effective de Sitter length ℓ_{dS} .

Before presenting our method in detail, we introduce two standard mathematical notions that we use extensively in our method: the dual triangulation and the triangulation geodesic distance. Given a causal triangulation (or, indeed, any triangulation), one constructs its dual in two steps: first place a dual vertex \tilde{s} at the geometric center of each D -simplex s ; then connect \tilde{s} and \tilde{s}' with a dual edge $\tilde{e}_{\tilde{s}\tilde{s}'}$ if and only if s and s' are nearest-neighbor D -simplices. In figure 3 we display the dual of the part of the 2-dimensional causal triangulation depicted in figure 1. As figure 3 shows, a dual triangulation is itself not

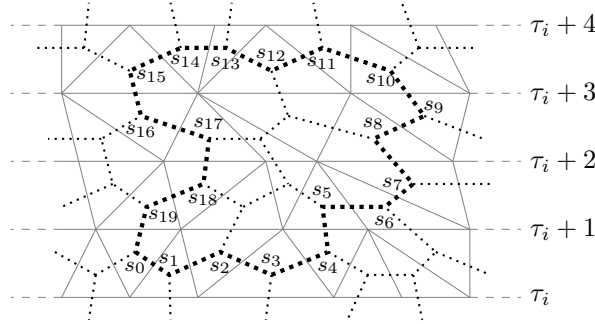


Figure 3: The dual of the part of the 2-dimensional causal triangulation of figure 1 shown in dotted lines. The thick dotted lines indicate a representative random walk starting from and returning to the 2-simplex s_0 .

necessarily a triangulation. One may also conceive of a dual causal triangulation as an abstract mathematical graph. Since the D -simplices employed in constructing causal triangulations are not regular, and since every D -simplex has $D+1$ nearest-neighbor D -simplices, the dual is a weighted $(D+1)$ -valent graph. (Of course, one may also conceive of a causal triangulation as an abstract mathematical graph, weighted and polyvalent.) We choose to work with the dual causal triangulation because dual vertices correspond to D -simplices, rendering diffusion a process along dual edges.

As a random walker diffuses, hopping from D -simplex to D -simplex along dual edges, it delineates a path P through the causal triangulation. Let $P\{s, \dots, s'\}$ be a path from s to s' , a string of D -simplices. The triangulation distance $d(P\{s, \dots, s'\})$ of $P\{s, \dots, s'\}$ is the sum of the lengths of the path's dual edges. Denoting by $N_{\tilde{e}_{(p,q)}^{(u,v)}}(P\{s, \dots, s'\})$ the number of dual edges connecting a (p, q) D -simplex

and a (u, v) D -simplex along $P\{s, \dots, s'\}$ and by $d(\tilde{e}_{(p,q)}^{(u,v)})$ the length of a dual edge connecting a (p, q) D -simplex and a (u, v) D -simplex,

$$d(P\{s, \dots, s'\}) = \sum_{\substack{(p,q) \\ (u,v)}} N_{\tilde{e}_{(p,q)}^{(u,v)}}(P\{s, \dots, s'\}) d(\tilde{e}_{(p,q)}^{(u,v)}). \quad (10)$$

If a causal triangulation were regular, then $d(P\{s, \dots, s'\})$ would simply be the number of dual edges along $P\{s, \dots, s'\}$ multiplied by the lattice spacing a (multiplied by a number of order 1). Causal triangulations are not in general regular because $d(\tilde{e}_{(p,q)}^{(u,v)})$ depends on the types of D -simplices. For our choice of $\alpha = 1$, however, $d(\tilde{e}_{(p,q)}^{(u,v)}) = \frac{a}{\sqrt{6}}$ irrespective of the types of 3-simplices. The triangulation geodesic distance $d_g(s, s')$ between s and s' is the minimum of $d(P\{s, \dots, s'\})$ over the set $\{P\{s, \dots, s'\}\}$ of paths between s and s' :

$$d_g(s, s') = \min_{\{P\{s, \dots, s'\}\}} d(P\{s, \dots, s'\}). \quad (11)$$

Intuitively, $d_g(s, s')$ is the shortest distance (in units of a) along dual edges from s to s' .

We now explain the first part of our method in which we establish the lattice distance associated with the diffusion time σ . A walk that returns to its starting D -simplex forms a cycle C in $\tilde{\mathcal{T}}_c$. Consider a cycle $C\{s_0, s_1, \dots, s_{\sigma-1}\}$ of σ steps starting and ending at s_0 . (Note that we do not include $s_\sigma = s_0$ in our notation for a cycle.) We associate a distance $\bar{d}_g(C\{s_0, s_1, \dots, s_{\sigma-1}\})$ to $C\{s_0, s_1, \dots, s_{\sigma-1}\}$ as follows. We compute $d_g(s_0, s_k)$ for $k \in \{0, 1, \dots, \sigma-1\}$, and we average $d_g(s_0, s_k)$ over these k :

$$\bar{d}_g(C\{s_0, s_1, \dots, s_{\sigma-1}\}) = \frac{1}{\sigma} \sum_{k=0}^{\sigma-1} d_g(s_0, s_k). \quad (12)$$

For the random walk depicted in figure 3, we list the distances $d_g(s_0, s_k)$ for $k \in \{0, 1, \dots, 19\}$ in table 1. $\bar{d}_g(C\{s_0, s_1, \dots, s_{\sigma-1}\})$ is the random walker's average triangulation geodesic distance from its starting D -simplex; $\bar{d}_g(C\{s_0, s_1, \dots, s_{\sigma-1}\})$ quantifies the typical lattice scale probed by the random walker diffusing along $C\{s_0, s_1, \dots, s_{\sigma-1}\}$.

As many cycles contribute to the heat kernel element $\mathcal{K}_{\mathcal{T}_c}(s_0, s_0, \sigma)$, we associate a distance $\bar{d}_g(s_0, \sigma)$ to s_0 by averaging $\bar{d}_g(C\{s_0, s_1, \dots, s_{\sigma-1}\})$ over these $N(C\{s_0, \sigma\})$ cycles:

$$\begin{aligned} \bar{d}_g(s_0, \sigma) &= \frac{1}{N(C\{s_0; \sigma\})} \\ &\times \sum_{j=1}^{N(C\{s_0; \sigma\})} \bar{d}_g(C_j\{s_0, s_1, \dots, s_{\sigma-1}\}). \end{aligned} \quad (13)$$

σ	d_g	σ	d_g	σ	d_g	σ	d_g
0	0	5	5	10	8	15	5
1	1	6	6	11	7	16	4
2	2	7	7	12	6	17	3
3	3	8	6	13	7	18	2
4	4	9	7	14	6	19	1

Table 1: The triangulation geodesic distances d_g of the random walker from its starting simplex s_0 in units of $a/\sqrt{6}$ as a function of the diffusion time σ for the random walk depicted in figure 3.

As many D -simplices contribute to the return probability $\mathcal{P}_{\mathcal{T}_c}(\sigma)$, we associate a distance $\bar{d}_g(\sigma)$ to \mathcal{T}_c by averaging over all $N_s(\mathcal{T}_c)$ simplices:

$$\bar{d}_g(\sigma) = \frac{1}{N_s(\mathcal{T}_c)} \sum_{s_0=1}^{N_s(\mathcal{T}_c)} \bar{d}_g(s_0, \sigma). \quad (14)$$

We estimate the expectation value $\mathbb{E}[\bar{d}_g(\sigma)]$ of $\bar{d}_g(\sigma)$ by the ensemble average $\langle \bar{d}_g(\sigma) \rangle$. $\langle \bar{d}_g(\sigma) \rangle$ is the distance in units of a that we associate to σ for random walks contributing to the ensemble average spectral dimension $\langle \mathcal{D}_s(\sigma) \rangle$.

The number of cycles, particularly nonsimple cycles, increases tremendously with the diffusion time, so we cannot possibly consider all cycles. To sample cycles efficiently without bias, we explicitly run a computationally reasonable number of random walks. Specifically, for each causal triangulation within an ensemble, we randomly sample of order 10^2 starting D -simplices, and, for each sampled starting D -simplex, we run of order 10^2 random walks. (Of course, only some of these walks form cycles, and this constitutes the primary inefficiency of our computations.) When estimating the error in our determination of $\langle \bar{d}_g(\sigma) \rangle$, we account for the errors stemming from these three levels of sampling.

In figure 4 we display a measurement of $\langle \bar{d}_g(\sigma) \rangle$. By inverting $\langle \bar{d}_g(\sigma) \rangle$, we determine the scale corresponding to σ in units of a . The analysis leading to figure 4 constitutes our primary innovation.

We next explain the second part of our method in which we relate the lattice spacing a to two physical length scales—the Planck length ℓ_P and the quantum geometry’s effective de Sitter length ℓ_{dS} —through the analysis first performed for $D = 4$ in [3] and subsequently performed for $D = 3$ in [19]. These authors analyzed the evolution of the discrete spatial D -volume in the distinguished foliation as quantified by the number N_{D-1}^{SL} of spacelike $(D - 1)$ -simplices as a function of the discrete time coordinate τ . In figure 5 we display $\langle N_2^{\text{SL}}(\tau) \rangle$ (in blue). Defining the

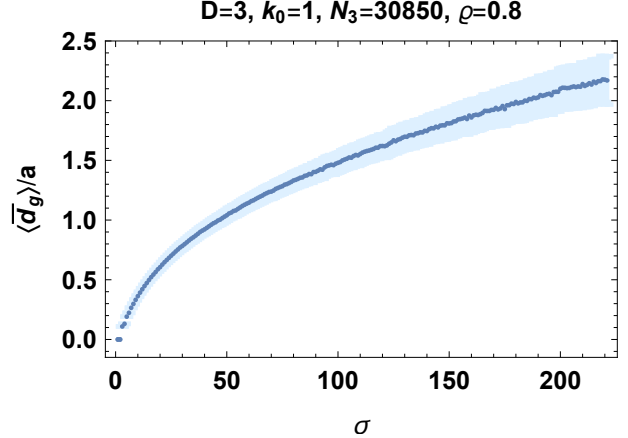


Figure 4: The ensemble average geodesic distance $\langle \bar{d}_g \rangle$ in units of the lattice spacing a as a function of the diffusion time σ (in blue). Each point’s vertical extent (in light blue) indicates its statistical error.

perturbation

$$\delta N_2^{\text{SL}}(\tau) = N_2^{\text{SL}}(\tau) - \langle N_2^{\text{SL}}(\tau) \rangle, \quad (15)$$

we display in figure 6 the first four eigenvectors of $\langle \delta N_2^{\text{SL}}(\tau) \delta N_2^{\text{SL}}(\tau') \rangle$ (in blue), and we display in figure 7 the eigenvalues of $\langle \delta N_2^{\text{SL}}(\tau) \delta N_2^{\text{SL}}(\tau') \rangle$ (in blue).

Following [19] in particular, we model $\langle N_2^{\text{SL}}(\tau) \rangle$ and $\langle \delta N_2^{\text{SL}}(\tau) \delta N_2^{\text{SL}}(\tau') \rangle$ on the basis of a minisuperspace truncation of the Euclidean Einstein-Hilbert action

$$S_{\text{EH}}^{(\text{E})}[V_2] = \frac{1}{32\pi G} \int_{t_i}^{t_f} dt \sqrt{g_{tt}} \left[\frac{\dot{V}_2^2(t)}{g_{tt} V_2(t)} - 4\Lambda V_2(t) \right] \quad (16)$$

(for nonstandard overall sign). G is the renormalized Newton constant, equivalent (for $D = 3$) to ℓ_P/\hbar , and Λ is the renormalized cosmological constant. To make direct contact with our measurements of $N_2^{\text{SL}}(\tau)$, we express the action (16) in terms of the spatial 2-volume V_2 (as opposed to the scale factor) as a function of the global time coordinate t . $\sqrt{g_{tt}}$ is the constant tt -component of the metric tensor. The extremum of the action (16) is Euclidean de Sitter space for which

$$V_2^{(\text{EdS})}(t) = 4\pi \ell_{\text{dS}}^2 \cos^2 \left(\frac{\sqrt{g_{tt}} t}{\ell_{\text{dS}}} \right) \quad (17)$$

with $t \in [-\pi \ell_{\text{dS}}/2\sqrt{g_{tt}}, +\pi \ell_{\text{dS}}/2\sqrt{g_{tt}}]$ and $\ell_{\text{dS}} = \Lambda^{-1/2}$. ℓ_{dS} is the de Sitter length. Expanding the action (16) to second order in the perturbation $\delta V_2(t)$

about the solution (17),

$$\begin{aligned}
S_{\text{EH}}^{(\text{E})}[\delta V_2] &= S_{\text{EH}}^{(\text{E})}[V_2^{(\text{EdS})}] \\
&+ \int_{t_i}^{t_f} dt \int_{t'_i}^{t'_f} dt' \delta V_2(t) K(t, t') \delta V_2(t') \quad (18) \\
&+ O[(\delta V_2)^3]
\end{aligned}$$

with

$$\begin{aligned}
K(t, t') &= -\frac{\sqrt{g_{tt}}\delta(t-t')}{64\pi^2 G \ell_{\text{dS}}^4} \sec^2\left(\frac{\sqrt{g_{tt}t}}{\ell_{\text{dS}}}\right) \left[\frac{\ell_{\text{dS}}^2}{g_{tt}} \frac{d^2}{dt^2} \right. \\
&+ \frac{2\ell_{\text{dS}}}{\sqrt{g_{tt}}} \sec\left(\frac{\sqrt{g_{tt}t}}{\ell_{\text{dS}}}\right) \tan\left(\frac{\sqrt{g_{tt}t}}{\ell_{\text{dS}}}\right) \frac{d}{dt} \\
&\left. + 2 \sec^2\left(\frac{\sqrt{g_{tt}t}}{\ell_{\text{dS}}}\right) \right]. \quad (19)
\end{aligned}$$

$K(t, t')$ is the van Vleck-Morette determinant [13]. A standard calculation of the expectation value $\mathbb{E}[\delta V_2(t) \delta V_2(t')]$ demonstrates that

$$\mathbb{E}[\delta V_2(t) \delta V_2(t')] = \hbar K^{-1}(t, t'). \quad (20)$$

This model makes contact with numerical measurements of $N_2^{\text{SL}}(\tau)$ through the double scaling limit

$$V_3 = \lim_{\substack{N_3 \rightarrow \infty \\ a \rightarrow 0}} C_3 N_3 a^3 \quad (21)$$

for the spacetime 3-volume V_3 [3, 9, 11, 19, 20]. In the combination of the thermodynamic ($N_3 \rightarrow \infty$) and continuum ($a \rightarrow 0$) limits, the product $C_3 N_3 a^3$ approaches a constant, namely V_3 . (For $\alpha = 1$, $C_3 = \frac{1}{6\sqrt{2}}$, the dimensionless discrete spacetime 3-volume of a 3-simplex.) Using the double scaling limit (21) and the solution (17), Anderson *et al* [11], following [3], derived the discrete analogue $\mathcal{V}_2^{(\text{EdS})}(\tau)$ of the solution (17):

$$\mathcal{V}_2^{(\text{EdS})}(\tau) = \frac{2\langle N_3 \rangle}{\pi \omega \langle N_3 \rangle^{1/3}} \cos^2\left(\frac{\tau}{\omega \langle N_3 \rangle^{1/3}}\right) \quad (22)$$

in which

$$\omega = \frac{\ell_{\text{dS}}}{\sqrt{g_{tt}} V_3^{1/3}}. \quad (23)$$

In figure 5 we display $\mathcal{V}_2^{(\text{EdS})}(\tau)$ (in black) fit to $\langle N_2^{\text{SL}}(\tau) \rangle$ (in blue). This first fit determines the value of ω . Using the double scaling limit (21) and the propagator (20), Cooperman, Lee, and Miller [19], following [3], derived the discrete analogue $\langle \delta \mathcal{V}_2(\tau) \delta \mathcal{V}_2(\tau') \rangle$ of the propagator (20). In figure 6 we display the first four eigenvectors of $\langle \delta \mathcal{V}_2(\tau) \delta \mathcal{V}_2(\tau') \rangle$ (in black) fit to the first four eigenvectors of $\langle \delta N_2^{\text{SL}}(\tau) \delta N_2^{\text{SL}}(\tau') \rangle$ (in blue). This sec-

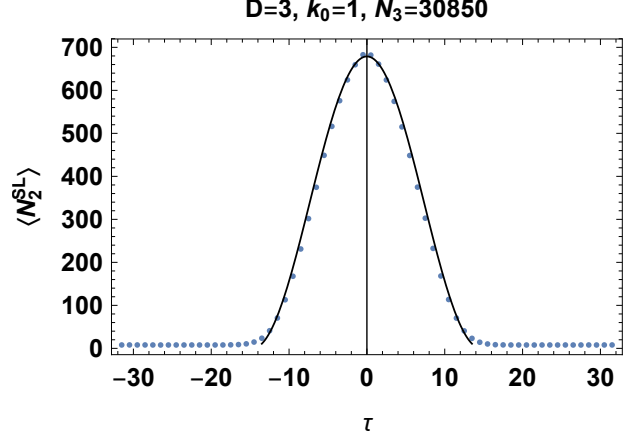


Figure 5: The ensemble average number $\langle N_2^{\text{SL}} \rangle$ of spacelike 2-simplices as a function of the discrete time coordinate τ (in blue) overlain with the best fit discrete analogue $\mathcal{V}_2(\tau)$ (in black). Statistical errors are not visible at this plot's scale.

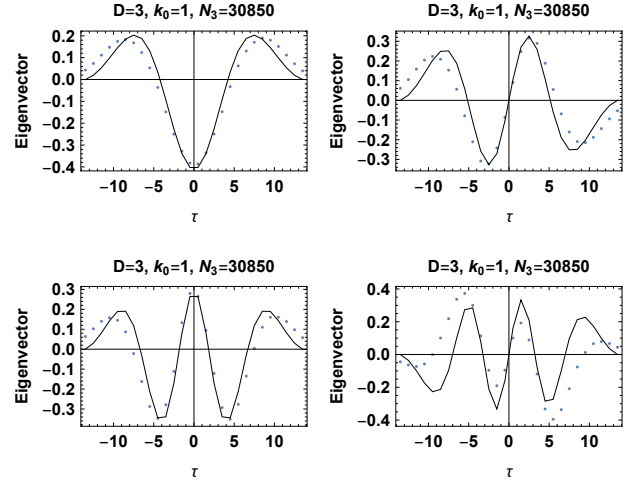


Figure 6: The first four eigenvectors (in blue) of $\langle \delta N_2^{\text{SL}}(\tau) \delta N_2^{\text{SL}}(\tau') \rangle$ overlain with the first four eigenvectors (in black) of the discrete analogue $\langle \delta \mathcal{V}_2(\tau) \delta \mathcal{V}_2(\tau') \rangle$. Statistical errors are not visible at this plot's scale.

ond fit takes as input the value of ω determined by the first fit and involves no further fit parameters. In figure 7 we display the eigenvalues of $\langle \delta \mathcal{V}_2(\tau) \delta \mathcal{V}_2(\tau') \rangle$ (in black) fit to the eigenvalues of $\langle \delta N_2^{\text{SL}}(\tau) \delta N_2^{\text{SL}}(\tau') \rangle$ (in blue). This third fit also takes as input the value of ω determined by the first fit and also requires the ratio r of the (largest) eigenvalue of $\langle \delta N_2^{\text{SL}}(\tau) \delta N_2^{\text{SL}}(\tau') \rangle$ to the (largest) eigen-

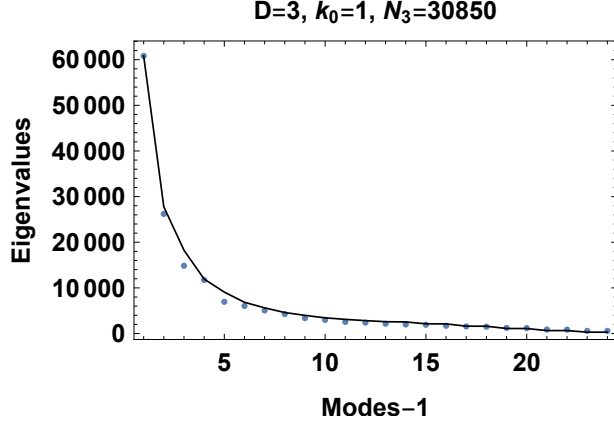


Figure 7: The eigenvalues of $\langle \delta N_2^{\text{SL}}(\tau) \delta N_2^{\text{SL}}(\tau') \rangle$ (in blue) overlap with the eigenvalues (in black) of the discrete analogue $\langle \delta \mathcal{V}_2(\tau) \delta \mathcal{V}_2(\tau') \rangle$. Statistical errors are not visible at this plot's scale.

value of $\langle \delta \mathcal{V}_2(\tau) \delta \mathcal{V}_2(\tau') \rangle$. All of these fits improves as N_3 increases [20]. These fits constitute the primary evidence that the quantum spacetime geometry on sufficiently large scales of the de Sitter phase is that of Euclidean de Sitter space.

Euclidean de Sitter space has spacetime 3-volume $V_3^{\text{(EdS)}} = 2\pi^2 \ell_{\text{dS}}^3$. Substituting $V_3^{\text{(EdS)}}$ for V_3 in the double scaling limit (21) (assumed to hold for finite N_3 and a with negligible corrections), one obtains the relationship

$$a = \left(\frac{2\pi^2}{C_3 N_3} \right)^{1/3} \ell_{\text{dS}} \quad (24)$$

between a and ℓ_{dS} . $\mathbb{E}[\delta V_2(t) \delta V_2(t')]$ has eigenvalues proportional to $64\pi^2 \hbar G \ell_{\text{dS}}^4 / \sqrt{g_{tt}}$. Relating the eigenvalues of $\mathbb{E}[\delta V_2(t) \delta V_2(t')]$ to the eigenvalues of $\langle \delta N_2^{\text{SL}}(\tau) \delta N_2^{\text{SL}}(\tau') \rangle$ through the double scaling limit (21), and using equations (23) and (24), one obtains the relationship

$$a = \frac{32N_3^{2/3}}{C_3^{1/3} \omega r} \ell_{\text{P}} \quad (25)$$

between a and ℓ_{P} . Having determined σ in units of a through our method's first part, we now use equation (24) or equation (25) to express a in units of ℓ_{dS} or ℓ_{P} , finally giving us the ensemble average spectral dimension $\langle \mathcal{D}_s \rangle$ as a function of a physical scale.

Results—For the ensemble of causal triangulations that we consider, $\omega = 0.2978$ and $r = 0.0000948$ both with negligible statistical error. Equation (24) becomes

$$a = 0.176 \ell_{\text{dS}}, \quad (26)$$

and equation (25) becomes

$$a = 20.46 \ell_{\text{P}}. \quad (27)$$

Consistent with previous studies, our simulations do not yet probe physical scales below ℓ_{P} .

In figure 8 we display the ensemble average spectral dimension $\langle \mathcal{D}_s \rangle$ as a function of physical scale in units of the Planck length ℓ_{P} and in units of the effective de Sitter length ℓ_{dS} . $\langle \mathcal{D}_s \rangle$ attains its maximum

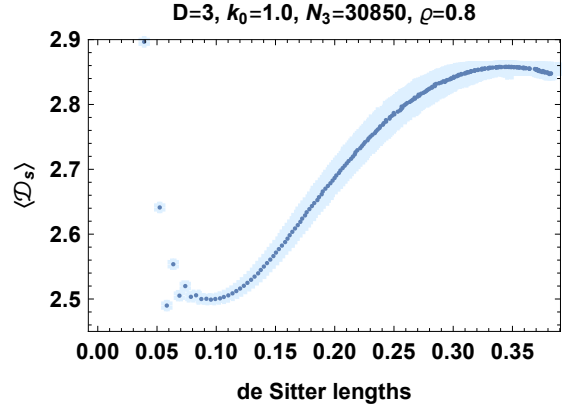
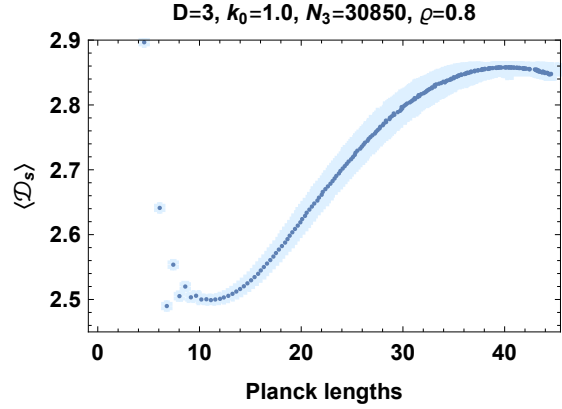


Figure 8: The ensemble average spectral dimension $\langle \mathcal{D}_s \rangle$ as a function of physical scale in units of the Planck length ℓ_{P} (top) and in units of the effective de Sitter length ℓ_{dS} (bottom). Each points' horizontal and vertical extents (in light blue) indicate its statistical error.

(depressed below the topological value of 3 by finite-size effects) at the physical scale of $40\ell_{\text{P}}$ or $0.34\ell_{\text{dS}}$. Dynamical reduction of $\langle \mathcal{D}_s \rangle$ then extends at least to a physical scale of $10\ell_{\text{P}}$ or $0.10\ell_{\text{dS}}$.

Conclusion—Through a conceptually straightforward but computationally intensive method, we have

established the physical scales over which dynamical reduction of the spectral dimension occurs within the de Sitter phase of causal dynamical triangulations. Our analysis demonstrates that this quantum-gravitational phenomenon begins to occur on physical scales more than an order of magnitude above the Planck length ℓ_P . Our analysis also demonstrates that the spectral dimension attains the value of the topological dimension D on a physical scale of $40\ell_P$. That the spectral dimension agrees with this value plausibly implies that the quantum spacetime geometry becomes semiclassical on this scale. Such an inference dictates that the quantum spacetime geometry within the de Sitter phase of causal dynamical triangulations is already semiclassical on scales only one order of magnitude above ℓ_P . Benedetti and Henson’s analysis of the spectral dimension indicates that this quantum spacetime geometry is not yet classical on this scale: they found that the ensemble average spectral dimension $\langle \mathcal{D}_s(\sigma) \rangle$ only begins to match the spectral dimension of Euclidean de Sitter space on a somewhat larger scale [12]. When combined with our method, Benedetti and Henson’s analysis would allow for the determination of the physical scale above which $\langle \mathcal{D}_s(\sigma) \rangle$ coincides with its classical value and for an independent determination of the quantum geometry’s effective de Sitter length ℓ_{dS} .

Ambjørn, Jurkiewicz, and Loll suggested that ℓ_P is the physical scale governing dynamical reduction of the spectral dimension [8]. These authors’ suggestion arose from their fit of a phenomenological 3-parameter function $D_s(\sigma; \alpha, \beta, \gamma)$ to $\langle \mathcal{D}_s(\sigma) \rangle$. The dimensionless parameter α sets $D_s(\sigma; \alpha, \beta, \gamma)$ to (approximately) 4 in the limit of large diffusion times; the dimensionless parameter β sets $D_s(\sigma; \alpha, \beta, \gamma)$ to (approximately) 2 in the limit of small diffusion times; and the dimensionful parameter γ determines the rate at which $D_s(\sigma; \alpha, \beta, \gamma)$ dynamically reduces from 4 to 2. Noting that γ divides the diffusion time σ , which itself has dimensions of length squared, they identified γ with ℓ_P^2 . We interpret Ambjørn, Jurkiewicz, and Loll’s ensuing discussion as an argument intended to bolster the identification of γ with ℓ_P^2 . These authors’ made two observations. First, they estimated the spacetime 4-volume V_4 of a causal triangulation in their ensemble as $N_4\ell_P^4$. We presume that they drew on the double scaling limit

$$V_4 = \lim_{\substack{N_4 \rightarrow \infty \\ a \rightarrow 0}} C_4 N_4 a^4, \quad (28)$$

the equivalent of equation (21) for $D = 4$. Setting $\ell_P = C_4^{1/4}a$ is then an implicit assumption. Taking the fourth root of $N_4\ell_P^4$ yielded approximately $20\ell_P$ for such a causal triangulation’s linear size. Second,

recalling that σ has dimensions of length squared, they estimated a random walker’s linear diffusion depth on a causal triangulation in their ensemble as $\sqrt{\sigma}\ell_P$. That one diffusion time step corresponds to a distance ℓ_P is essentially the same implicit assumption. Considering the diffusion time σ_{max} at which $\langle \mathcal{D}_s(\sigma) \rangle$ attains a value of 4 yielded approximately $20\ell_P$ for such a causal triangulation’s linear diffusion depth. We presume that they chose to consider σ_{max} on the basis of the previous paragraph’s reasoning that the quantum spacetime geometry is plausibly (at least) semiclassical on the scale at which $\langle \mathcal{D}_s(\sigma) \rangle$ attains a value of 4. We take Ambjørn, Jurkiewicz, and Loll’s two observations to imply the argument’s unstated conclusion: the (approximate) equality of the two estimates constitutes evidence for the validity of the identification of ℓ_P with the physical scale governing dynamical reduction of the spectral dimension.

Our above analysis as well as the analyses of Ambjørn *et al* [3] and Benedetti and Henson [12] inform the previous paragraph’s argument. The implicit assumption—that $\ell_P = C_4^{1/4}a$ —yields $\ell_P \approx \frac{1}{2}a$ for typical values of C_4 . In combination with the double scaling limit (28) and the spacetime 4-volume of Euclidean de Sitter space, the estimate of V_4 yields $\ell_{\text{dS}} \approx 3a$. Ambjørn *et al*’s more detailed analysis corroborates these estimates [3]. Ambjørn, Jurkiewicz, and Loll’s estimate of the linear diffusion depth then dictates that $\langle \mathcal{D}_s(\sigma) \rangle$ attains a value of 4 on a scale of approximately $3\ell_{\text{dS}}$. This value is an order of magnitude greater than the same scale’s value, $0.34\ell_{\text{dS}}$, within our simulations. Moreover, Benedetti and Henson’s analysis suggests that σ reaches the scale ℓ_{dS} well beyond σ_{max} , the value of σ at which $\langle \mathcal{D}_s(\sigma) \rangle$ attains the value D [12]. One might therefore suspect that estimating the linear diffusion depth as $\sqrt{\sigma}$ —the scaling for Euclidean space—is simply too naive; however, our measurement of the ensemble average geodesic distance $\langle \bar{d}_g(\sigma) \rangle$ justifies this estimate. Fitting the function $\kappa\sigma^\eta$ to $\langle \bar{d}_g(\sigma) \rangle$ yields $\kappa = 0.157 \pm 0.001$ and $\eta = 0.488 \pm 0.002$ for these two parameters. In figure 9 we display $\kappa\sigma^\eta$ (in black) fit to $\langle \bar{d}_g(\sigma) \rangle$ (in blue). The plot in figure 9 shows that $\langle \bar{d}_g(\sigma) \rangle$ increases with σ very nearly as $\sqrt{\sigma}$ except for sufficiently small σ . We have thus substantiated Ambjørn, Jurkiewicz, and Loll’s estimates.

While $N_4^{1/4}\ell_P$ and $\sqrt{\sigma_{\text{max}}}\ell_P$ agree for the ensemble of 4-dimensional causal triangulations that Ambjørn, Jurkiewicz, and Loll considered, $N_3^{1/3}\ell_P$ and $\sqrt{\sigma_{\text{max}}}\ell_P$ disagree by an order of magnitude for the ensemble of 3-dimensional causal triangulations that we consider. The argument based on the approx-

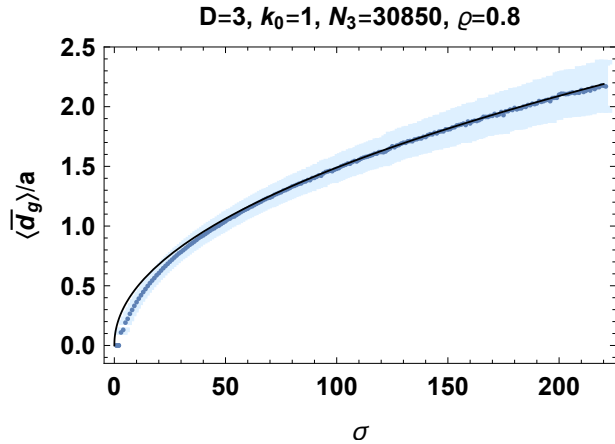


Figure 9: The ensemble average geodesic distance $\langle \bar{d}_g \rangle$ in units of the lattice spacing a as a function of the diffusion time σ (in blue) overlain with the best fit function $\kappa \sigma^n$ (in black). Each point’s vertical extent (in light blue) indicates its statistical error.

imate equality of $N_D^{1/D} \ell_P$ and $\sqrt{\sigma_{\max}} \ell_P$ breaks down for $D = 3$, and we now doubt that this argument holds generally for $D = 4$. This breakdown notwithstanding, we can lend new support to Ambjørn, Jurkiewicz, and Loll’s suggestion that ℓ_P governs dynamical reduction of the spectral dimension. Above we have unveiled the following picture: within simulations studied so far for $D = 3$, dynamical reduction of $\langle \mathcal{D}_s(\sigma) \rangle$ occurs over scales of order $10\ell_P$ or $10^{-1}\ell_{\text{dS}}$, and, within simulations studied so far for $D = 4$, dynamical reduction of $\langle \mathcal{D}_s(\sigma) \rangle$ occurs over scales of order $10\ell_P$ or ℓ_{dS} . The physical scale characterizing dynamical reduction of $\langle \mathcal{D}_s(\sigma) \rangle$ is independent of D when expressed in units of ℓ_P , which suggests that ℓ_P sets the scale of this quantum-gravitational phenomenon.

Cooperman first advocated that measurements of $\langle \mathcal{D}_s(\sigma) \rangle$ could form the basis for a renormalization group analysis of causal dynamical triangulations, and he proposed a method for performing such an analysis [16]. Subsequently, Ambjørn *et al* attempted to track relative changes in the lattice spacing across the de Sitter phase with measurements of $\langle \mathcal{D}_s(\sigma) \rangle$ [1]. These authors employed a different method, which Cooperman criticized [17]. Our above analysis, when combined with Cooperman’s scaling analysis of the spectral dimension [18], should allow for the realization of Cooperman’s original proposal. We hope that our analysis thereby aids the search for a continuum limit of causal dynamical triangulations effected by a nontrivial ultraviolet fixed point of the renormaliza-

tion group.

Acknowledgements—We thank Christian Anderson, Jonah Miller, and especially Rajesh Kommu for allowing us to employ parts of their codes. We also thank Steve Carlip, Hal Haggard, and Jonah Miller for useful discussions. We acknowledge the hospitality and support of the Physics Program of Bard College where we completed much of this research.

References

- [1] J. Ambjørn, D. N. Coumbe, J. Gizbert-Studnicki, and J. Jurkiewicz. “Searching for a continuum limit of causal dynamical triangulation quantum gravity.” *Physical Review D* 93 (2016) 104032.
- [2] J. Ambjørn, A. Görlich, J. Jurkiewicz, A. Kreienbuehl, and R. Loll. “Renormalization group flow in CDT.” *Classical and Quantum Gravity* 31 (2014) 165003.
- [3] J. Ambjørn, A. Görlich, J. Jurkiewicz, and R. Loll. “Nonperturbative quantum de Sitter universe.” *Physical Review D* 78 (2008) 063544.
- [4] J. Ambjørn, A. Görlich, J. Jurkiewicz, and R. Loll. “Nonperturbative quantum gravity.” *Physics Reports* 519 (2012) 127.
- [5] J. Ambjørn, J. Jurkiewicz, and R. Loll. “Nonperturbative Lorentzian Path Integral for Gravity.” *Physical Review Letters* 85 (2000) 347.
- [6] J. Ambjørn, J. Jurkiewicz, and R. Loll. “Dynamically triangulating Lorentzian quantum gravity.” *Nuclear Physics B* 610 (2001) 347.
- [7] J. Ambjørn, J. Jurkiewicz, and R. Loll. “Nonperturbative 3d Lorentzian Quantum Gravity.” *Physical Review D* 64 (2001) 044011.
- [8] J. Ambjørn, J. Jurkiewicz, and R. Loll. “The Spectral Dimension of the Universe is Scale Dependent.” *Physical Review Letters* 95 (2005) 171301.
- [9] J. Ambjørn, J. Jurkiewicz, and R. Loll. “Reconstructing the universe.” *Physical Review D* 72 (2005) 064014.
- [10] J. Ambjørn and R. Loll. “Non-perturbative Lorentzian quantum gravity, causality, and topology change.” *Nuclear Physics B* 536 (1998) 407.

- [11] C. Anderson, S. Carlip, J. H. Cooperman, P. Hořava, R. K. Kommu, and P. Zulkowski. “Quantizing Hořava-Lifshitz gravity via causal dynamical triangulations.” *Physical Review D* 85 (2012) 049904.
- [12] D. Benedetti and J. Henson. “Spectral geometry as a probe of quantum spacetime.” *Physical Review D* 80 (2009) 124036.
- [13] N. D. Birrell and P. C. W. Davies. *Quantum fields in curved space*. Cambridge University Press 1982.
- [14] S. Carlip. “Dimension and dimensional reduction in quantum gravity.” *Classical and Quantum Gravity* 34 (2017) 193001.
- [15] J. H. Cooperman. “Scale-dependent homogeneity measures for causal dynamical triangulations.” *Physical Review D* 90 (2014) 124053.
- [16] J. H. Cooperman. “On a renormalization group scheme for causal dynamical triangulations.” *General Relativity and Gravitation* 48 (2016) 1.
- [17] J. H. Cooperman. “Comments on ‘Searching for a continuum limit in CDT quantum gravity’.” arXiv: 1604.01798
- [18] J. H. Cooperman. “Scaling analyses of the spectral dimension in 3-dimensional causal dynamical triangulations.” *Classical and Quantum Gravity* 35 (2018) 105004.
- [19] J. H. Cooperman, K. Lee, and J. M. Miller. “A second look at transition amplitudes in $(2 + 1)$ -dimensional causal dynamical triangulations.” *Classical and Quantum Gravity* 34 (2017) 115008.
- [20] J. H. Cooperman and J. M. Miller. “A first look at transition amplitudes in $(2 + 1)$ -dimensional causal dynamical triangulations.” *Classical and Quantum Gravity* 31 (2014) 035012.
- [21] D. N. Coumbe and J. Jurkiewicz. “Evidence for asymptotic safety from dimensional reduction in causal dynamical triangulations.” *Journal of High Energy Physics* 03 (2015) 151.
- [22] R. K. Kommu. “A validation of causal dynamical triangulations.” *Classical and Quantum Gravity* 29 (2012) 105003.